

Occlusion-aware Hand Pose Estimation Using Hierarchical Mixture Density Network

Qi Ye, Tae-Kyun Kim
Imperial College London, UK
{q.ye14, tk.kim}@imperial.ac.uk

Abstract

Hand pose estimation is to predict the pose parameters representing a 3D hand model, such as locations of hand joints. This problem is very challenging due to large changes in viewpoints and articulations, and intense self-occlusions, etc. Many researchers have investigated the problem from both aspects of input feature learning and output prediction modelling. Though effective, most of the existing discriminative methods only give a deterministic estimation of target poses. Also, due to their single-value mapping intrinsic, they fail to adequately handle self-occlusion problems, where occluded joints present multiple modes. In this paper, we tackle the self-occlusion issue and provide a complete description of observed poses given an input depth image through a hierarchical mixture density network (HMDN) framework. In particular, HMDN leverages the state-of-the-art CNN module to facilitate feature learning, while proposes a density in a two-level hierarchy to reconcile single-valued and multi-valued mapping in the output. The whole framework is naturally end-to-end trainable with a mixture of two differentiable density functions. HMDN produces interpretable and diverse candidate samples, and significantly outperforms the state-of-the-art algorithms on benchmarks that exhibit occlusions.

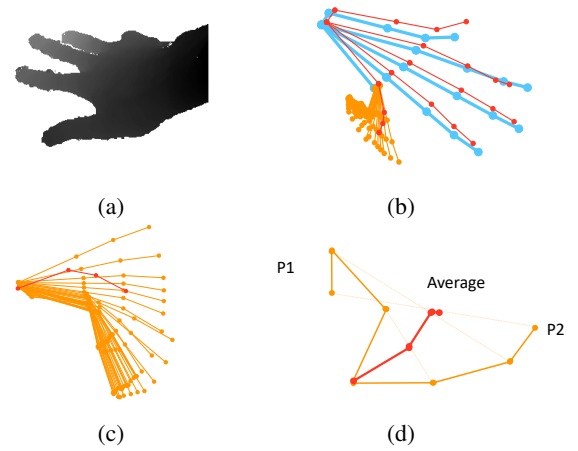


Figure 1: (a) A depth image with the pinky finger occluded. (b) Multiple ground truth pose labels for the image (occluded joints in yellow) and the estimated hand pose (in red) by a CNN trained using a sum-of-squares error. The hand poses are shown in 3D coordinates by changing the viewpoint to better illustrate the multiple labels for the occluded joints. (c) A closer look on the multiple ground truth and deterministic estimation for the occluded joints. (d) The average of two ground truth labels for the pinky finger gives a physically implausible pose.

1. Introduction

Hand pose estimation gains an increasing interest with the availability of commercial depth cameras and the need of applications in human-computer interactions, such as virtual reality (VR)[5], sign language recognition[3, 29], activity recognition[14]. Generally, there are two typical camera settings: third-person viewpoints, where the camera is set in front of a user and first-person (or egocentric) viewpoints, where the camera is mounted on the head (many VR glasses, for examples), or shoulder. Though in both settings the estimation shares some same challenges, like the full range of global rotations, complex articulations,

self-occlusions and self-similar parts of hands, the self-occlusions happen less frequently in third-viewpoints due to typical hand motions. For example, there are less than 9% of occluded finger joints in the two widely used benchmarks, ICVL[23] and NYU[24] respectively.

Most discriminative methods in hand pose estimation learn a mapping from an input image to its pose parameters, and perform well on the third-viewpoint setting. However, they fail to handle the occlusion problems frequently encountered in egocentric viewpoints. They treat the mapping to be single-valued without being aware that when occlusions occur, there may exist multiple pose hypotheses

for the input image. For the input image in Fig. 1a where the pinky finger is occluded, there are multiple ground truth pose labels in the BigHand dataset[30]. They are shown in yellow skeletons in Fig. 1b and Fig. 1c.

Given a set of hand images with 3D joint coordinate location labels, discriminative methods, convolutional neural networks (CNN) for example, minimize a sum-of-squares error function and the minimization of the error function outputs estimations which approximate the averages of the target locations conditioned on the input images. When all the joints in the input image are visible, the mapping is single-valued and the conditional average is correct, though the average only provides a limited description of the properties of the target locations. In the occlusion cases, however, which happen frequently in hand images and are particularly severe in the egocentric and hand-object interaction scenarios, the mapping is multi-valued due to the existence of multiple poses for the occluded joints. The conditional average of all the correct joint locations is not necessarily a correct estimation. The red skeleton in Fig. 1b shows a CNN estimation trained with the sum-of-squares error function. For the visible joints, the estimation is interpretable and close to the ground truth while for the occluded joints, the CNN gives an estimation physically implausible and not close to one of the given poses. This can be further clarified in the following. Assuming that the locations of joints on the finger have two possible configurations (P1 and P2 shown in Fig. 1d), if a CNN with a sum-of-squares error function is trained on two identical images but with two different ground truth labels, it gives the estimation in red in Fig. 1d, which is apparently not a plausible pose.

Further, CNN trained with the minimization of the sum-of-squares error not only outputs an average that may not be correct itself but also lacks of the description of the properties of the target joint locations. The discriminative method often serves as the initialisation of a generative method. For generative methods which search the entire pose space to find a best hypothesis that minimizes the discrepancy between the rendered image and the input image, a distribution that well fits the data not only reduces the search space and thus ensures a faster convergence but also avoids local minimas by providing diverse candidates. Combined with only the deterministic estimation of existing discriminative methods, however, the generative methods tend to be ignorant of the region to be explored ahead and also can not treat the optimization of visible joints and occluded joints separately.

In this paper, a hierarchical mixture density network (HMDN) is proposed to give a complete description of hand poses given images with occlusions by modelling conditional probability distributions of the target joint locations. The distribution for a joint is modelled in a two-level hierarchy to reconcile the single- and multi-valued mapping

problems conditioned on the visibility of the joint. The first level is a distribution for a latent variable representing the visibility of a joint and the second level is a distribution for the joint location dependent on the visibility: the visible joint represented by a single Gaussian kernel corresponding its single-valued mapping trait and the occluded joint represented by a mixture of multiple Gaussian kernels to fit the multi-valued mapping. To leverage CNN for effective feature learning, the hierarchical mixture density of the distribution is topped upon a CNN output layer and the whole framework can be trained end-to-end with the differentiable density function. To the best of our knowledge, the proposed HMDN is the first time that gives estimation by a conditional distribution with the awareness of occlusion in 3D hand pose estimation.

2. Related Work

2.1. Hand Pose Estimation

For free hand motions, the methods explicitly tackling the self-occlusions are rare as most existing datasets are collected in third-viewpoints and the proportions of occluded joints are small. Franziska *et al.* [8] point that many existing methods fail to work under occlusions and even commercial systems claiming for egocentric viewpoints often fail under large occlusions. However, there are some approaches working on hand-object interactions while dealing with the occlusions. Franziska *et al.* [8] and Rogez *et al.* [13, 12] use synthetic images for training a model for difficult egocentric views. Sridhar *et al.* [19, 17, 18] and Dimitrios *et al.* [25] exploit the estimation of the discriminative methods to aid the search of the generative methods. The discriminative methods used in these approaches are deterministic.

On the other hand, existing discriminative methods do not address multi-modalities nor do not model the difference in the data distribution for visible joints and occluded joints. For pose regression based on CNN, the loss of the methods[10, 9, 24, 28] is the sum-of-squares error, resulting in the issues we have discussed when occlusions exist. For regression based on random forests, as the estimation is made from the data in the leaf node, it is convenient to fit a multi-modal model to the data. However, with no information of which joints are visible or occluded, the data in all leaf nodes is modelled either by mean-shift [23, 20, 16] (uni-modal) or a Gaussian Mixture Model (GMM)[22].

2.2. Mixture Models

Mixture density network(MDN) is first proposed in [1] to enable neural network to produce distribution and overcome the limitation of the sum-of-squares error function. Zen *et al.* [31] use MDN for acoustic modelling and Kinoshita *et al.* [7] for speech feature enhancement. Variani[26] proposes to learn the feature for a GMM and the model jointly.

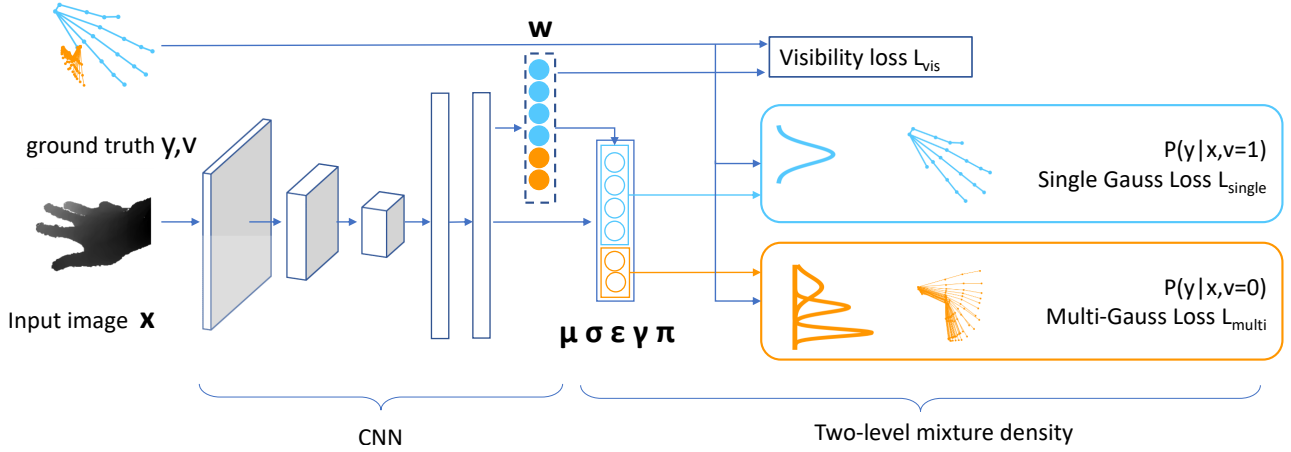


Figure 2: Hierarchical Mixture Density Network. The CNN outputs the parameters of the hierarchical mixture density, $w, \mu, \sigma, \epsilon, \gamma, \pi$. Depending on the visibility of a joint, a uni-modal Gaussian model or a GMM is chosen to model the target locations.

All these work only applies MDN to model acoustic signals without an adaptation of the mixture density model. Our paper not only applies MDN to hand pose estimation but also extends MDN by a two-level hierarchy to fit the specific mixture of single-valued and multi-valued problems. A similar hierarchical mixture model is proposed in [4] to represent "useful" data and "noise" by different sub-components and a Bayesian approach is used to learn the parameters of the mixture model. Different from the work, we model a conditional distribution and use a CNN to discriminatively learn the parameters of the model.

3. Model Representation

3.1. Hierarchical Mixture Density Network

We assume the generation of a hand depth image is controlled by two sets of parameters: one represents the pose parameter of a 3D hand model and the other generates a 2D image from the 3D hand model. The image formation is not simply by projecting each point of the 3D model onto the 2D image but also considers the decision of the visibility of each projected pixel in the 2D image. We simplify the generation of 2D image from the 3D hand model to be controlled by a vector that denotes whether the hand bones (than joints here) are visible not. Our problem, inverse of the process, is finding the configuration of the pose parameter given an image.

Let x be the hand image and y the 3D pose representing the hand model associated with the image. Each pose y represents a set of 3D locations for hand joints $\{y_i\}$, where $y_i \in R^3$, $i = 1, \dots, d$ and i indexes different hand joints. d joints are treated independently. i is also used to identify the bone associated with the i -th joint, hereinafter we use

the index for bones and joints interchangeably.

When a bone is visible, the joint location is deterministic and when a bone is occluded, there are usually multiple candidates for the joint location. In order to address this issue, we use a two-level mixture density model to represent y , by which we can switch between two cases and provide a full description of the target poses. Conditioned on an input image x , the pose y is drawn from two sub-components depending on the visibility: the first one that is a uni-modal distribution, generating locations for visible joints and the second subcomponent that is a multi-modal distribution, generates locations for joints under occlusion. As d hand joints are independent, to facilitate the explanation, for all the variables below we leave the subscript i . The distribution of y is conditioned on x , but for simplicity, we omit the condition x in the following.

First, a binary variable v is introduced to represent whether the joint is visible or not, which takes a Bernoulli distribution

$$p(v|w) = w^v(1-w)^{(1-v)} \quad (1)$$

When $v = 1$, the joint is visible in the image and the location is deterministic. Considering the label noise, we assume the pose y is generated from a uni-modal Gaussian distribution

$$p(y|\mu, \sigma, v = 1) = N(y; \mu, \sigma) \quad (2)$$

When a joint is occluded, *i.e.* $v = 0$, there are multiple hypotheses for the locations and thus we assume the pose is generated from a multi-modal distribution by a GMM with

J components, which is dependent on a hidden variable z .

$$p(y|z, \epsilon, \Gamma, v = 0) = \prod_{j=1}^J N(y; \epsilon_j, \gamma_j)^{z_j} \quad (3)$$

where $\epsilon = \{\epsilon_j\}$ and $\Gamma = \{\gamma_j\}$. z_j is one element of the J -dimensional latent variable z and the variable is a 1-of- J representation. If $z_j = 1$, the joint location is drawn from the j -th component. Assume the distribution of z has the form $p(z|\Pi) = \prod_{j=1}^J \pi_j^{z_j}$, where $0 \leq \pi_j \leq 1$ and $\sum_{j=1}^J \pi_j = 1$, equation (3) can be re-written as $p(y|\Pi, \epsilon, \Gamma, v = 0) = \sum_{j=1}^J \pi_j N(y; \epsilon_j, \gamma_j)$, where $\Pi = \{\pi_j\}$.

With all components defined, the distribution for y depending on v is

$$p(y|v, \mu, \sigma, \epsilon, \Gamma, \Pi) = [N(y; \mu, \sigma)]^v \left[\sum_{j=1}^J \pi_j N(y; \epsilon_j, \gamma_j) \right]^{(1-v)} \quad (4)$$

and the joint distribution of y and v is

$$p(y, v|w, \mu, \sigma, \epsilon, \Gamma, \Pi) = [wN(y; \mu, \sigma)]^v \left[(1-w) \sum_{j=1}^J \pi_j N(y; \epsilon_j, \gamma_j) \right]^{(1-v)} \quad (5)$$

Equation (4) shows that the generation of a pose y given the input image x is in two levels: first, a sample v is drawn from (1) and then depending on the value of v , a hypothesis is drawn either from a uni-modal Gaussian or a GMM. As v is not available during testing, the joint distribution (5) of v and y should be known to generate a pose.

The above distribution is for one joint y_i , so for the full pose, which consists of d independent joints, the distribution for the full pose is obtained by multiplying all the distributions of individual joints. For the observed full poses $Y = \{y^n\}$ for x , the likelihood of Y and visibility v of all joints given the parameters is $\prod_{n=1}^N \prod_{i=1}^d p(y_i^n, v_i | w_i, \mu_i, \sigma_i, \epsilon_i, \Gamma_i, \Pi_i)$ and our aim is to find the parameters conditioned to maximize the likelihood.

Note that the hierarchical mixture density (4) and the joint distribution (5) is conditioned on x . All the parameters $w_i, \mu_i, \sigma_i, \epsilon_i, \Gamma_i, \Pi_i$ should be dependent on the input image x accordingly, which are represented in a functional form, i.e. $w_i(x), \mu_i(x), \sigma_i(x), \epsilon_i(x), \Gamma_i(x), \Pi_i(x)$. The joint density (5) is differentiable, we choose the CNN to learn the functions for the parameters.

As shown in Fig. 2, the parameters are put in the output layer of the CNN, which are made up of three parts for each

joint: w_i for the visibility variable in (1), μ_i, σ_i for the uni-modal Gaussian in (2), and $\epsilon_i, \Gamma_i, \Pi_i$ for the GMM in (3). Different activation functions are used to force the outputs to satisfy the range of the parameters. For instance, σ is activated by an exponential function to remain a positive value and π by a softmax function to be in $[0, 1]$. Depending on the visibility prediction (the value of w), the parameters for the uni-modal Gaussian or GMM are chosen to compute the loss, which is depicted in two colours. For example, the joints on the pinky finger displayed in Fig. 2 are occluded according to the ground truth (or prediction), GMMs are chosen to compute the likelihood. For other joints, single Gaussian Models are chosen.

3.2. Training and Testing

Given a dataset with F images and labels for the location and the visibility of the joints, defined by the triplets $\{\{x, Y, v\}^f | f = 1 \dots F\}$, the likelihood over the whole dataset is

$$P = \prod_{f=1}^F \prod_{n=1}^N \prod_{i=1}^d p(y_i^{nf}, v_i^f | w_i^f, \mu_i^f, \sigma_i^f, \epsilon_i^f, \Gamma_i^f, \Pi_i^f) \quad (6)$$

where $w_i^f, \mu_i^f, \sigma_i^f, \epsilon_i^f, \Gamma_i^f, \Pi_i^f$ indicate the parameters dependent on the frame x^f . Thus, our goal is to learn the functions from the input images to the parameter configurations of the hierarchical mixture density by maximizing the likelihood on the dataset.

We use the negative logarithmic likelihood as our loss function,

$$L = \sum_{f=1}^F \sum_{n=1}^N \sum_{i=1}^d L_{vis} + L_{single} + L_{multi} \quad (7)$$

$$L_{vis} = -v_i^f \log(w_i^f) - (1 - v_i^f) \log(1 - w_i^f) \quad (8)$$

$$L_{single} = -v_i^f \log(N(y_i^{nf}; \mu_i^f, \sigma_i^f)) \quad (9)$$

$$L_{multi} = -(1 - v_i^f) \log\left(\sum_{j=1}^J \pi_{ij}^{nf} N(y_{ij}^{nf}; \epsilon_{ij}^f, \gamma_{ij}^f)\right) \quad (10)$$

where the three loss functions correspond to the three branches in Fig. 2.

During testing, when an image x is fed into the network, the prediction for the i -th joint location is diverted to different branches according to the prediction of the visibility of the joint. If w_i is larger than 0.5, the prediction (or sampling) for the location is made by the uni-modal Gaussian distribution; otherwise, the GMM. However, when the prediction for the visibility is erroneous, the prediction for the location will be wrong, as during training, the parameters for the uni-modal Gaussian distribution have not seen samples for occluded joints and also the parameters for

GMM have not accounted samples for visible joints. This introduces a bias as during testing: the visibility variable is drawn from the predicted distribution, which is different from that in training.

To help the bias problem, instead of maximizing the likelihood of the joint distribution using the visibility ground truth of joints, we use M samples $\{v'_m\}$ drawn from the estimated distribution (1) for the visibility variable v . Therefore, the v_i^f in (9)(10) is replaced by $\sum_{m=1}^M v'_{im}{}^f$, which equates w when M is large enough. So, the losses (9)(10) are changed into

$$L_{single} = w_i^f \log(N(y_i^{nf}; \mu_i^f, \sigma_i^f)) \quad (11)$$

$$L_{multi} = (1 - w_i^f) \log\left(\sum_{j=1}^J \pi_{ij}^{nf} N(y_{ij}^f; \varepsilon_{ij}^f, \gamma_{ij}^f)\right) \quad (12)$$

The modified losses (11)(12) can be seen as a soft version of the original ones (9)(10).

3.3. Degradation into Mixture Density Network

HMDN degrades into MDN without the supervision by the ground truth for learning the visibility variable. The other form of equation(4) is

$$p(y|w, \mu, \sigma, \varepsilon, \Gamma, \Pi) = wN(y; \mu, \sigma) + (1 - w) \left[\sum_{j=1}^J \pi_j N(y; \varepsilon_j, \gamma_j) \right] \quad (13)$$

which is re-written as

$$p(y|\epsilon', \Gamma', \Pi') = \sum_{j=1}^{J+1} \pi'_j N(y; \varepsilon'_j, \gamma'_j) \quad (14)$$

where $\pi'_{J+1} = w, \varepsilon'_{J+1} = \mu, \gamma'_{J+1} = \sigma$ and $\pi'_j = (1 - w)\pi_j, \varepsilon'_j = \varepsilon_j, \gamma'_j = \gamma_j, j = 1 \dots J$. Equation (14) is a GMM with $J+1$ component because w in (13), which is learnt by the supervision of target location, is absorbed into π' . Though can be written in the same mathematical form, HMDN and MDN have different physical meanings and exhibit differently according to the data.

4. Experiments

4.1. Datasets

Public benchmarks for hand pose estimation are collected mostly in third-viewpoints and do not offer plenty of occluded joints with multiple pose labels. We investigate the four datasets, ICVL [21], NYU [24], MSHD [16] and BigHand [30], and exploit those containing a higher portion of occluded joints. The proportion of occluded finger joints

and the number of training and testing images are listed in Table 1.

Table 1: Proportion of occluded finger joints and number of frames on four datasets

Dataset	Train(prop/frames)	Test(prop/frames)
ICVL	0.06 / 16,008	0.01 / 1,596
NYU	0.09 / 72,757	0.36 / 8,252
MSHD	0.33 / 100,000	0.16 / 2,000
EgoBigHand	0.48 / 969,600	0.53 / 649,536

For the BigHand dataset, we use the ego-centric subset, and part of the skeletons collected in third-viewpoint subset which exhibits abundant articulations are used to augment the modalities of occluded joints. The ego-centric subset consists of 9 subjects. We choose 2 subjects as a part of the testing set and randomly select clips of frames (each clip last to 10 seconds) captured from the other 7 subjects as the other part of the testing set. The remaining frames form the training set. This dataset is denoted as EgoBigHand, used for main experiments. More results are also shown on MSHD and NYU datasets.



Figure 3: Leftmost: the hand sphere model; Right: two examples with pixels assigned to different parts

The images in these datasets are only labelled with joint locations without the visibility information of hand parts. To get the visibility label for training HMDN and analysing the results w.r.t. occlusions, we use a sphere model similar to [11]. The sphere centres are inferred from the ground truth joint locations. The image pixels are assigned to the spheres according to their distance and hand parts whose spheres have the number of pixels below a threshold are found as occluded. Sphere model and examples of assigned pixels are shown in Fig. 3.

4.2. Self-comparisons

The CNN network used is the U-net proposed in [15], by adapting the final layers to fully connected layers for regression. All the networks are trained using Adam[6] and the best learning rate is searched for each network.

In the previous section, we showed that HMDN degrades to MDN, when there is no supervision on the latent visibility variables. MDN is one of our baselines. To compare MDN with HMDN fairly, the number of Gaussian kernels of MDN and HMDN is set the same, *i.e.* the number of

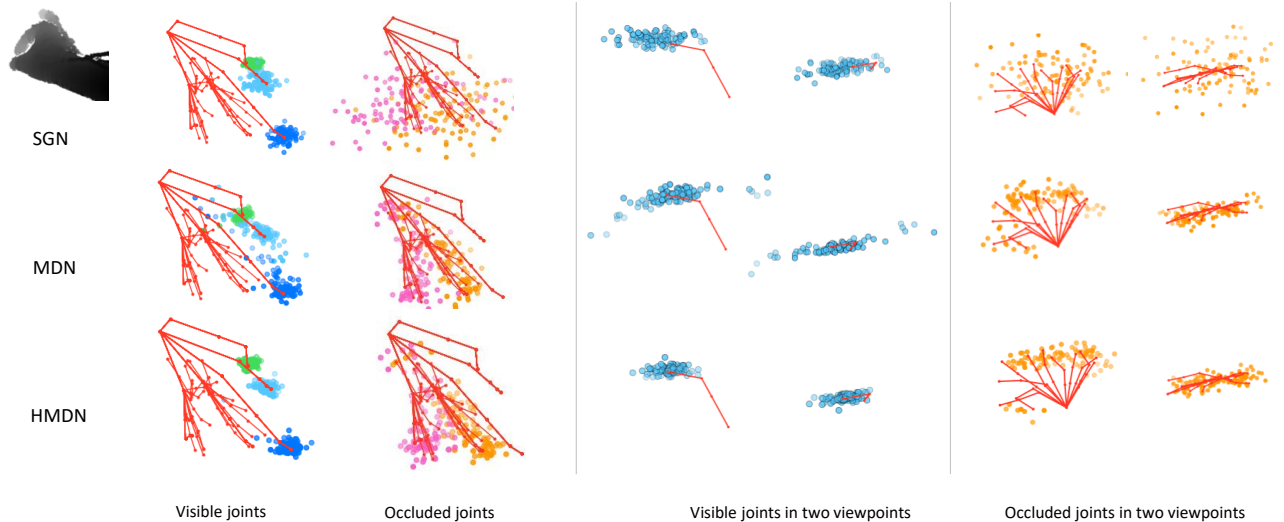


Figure 4: Left: samples drawn from distributions produced by SGN, MDN and HMDN. Middle: samples for visible index finger tip shown in two viewpoints. Right: samples for occluded ring finger tip shown in two viewpoints.

kernels of MDN is $J + 1$. The other baseline is the standard CNN trained with the least squares error. In [2], it is shown that maximization of the likelihood function under a uni-modal Gaussian distribution for a linear model is equivalent to minimizing a sum-of-squares error. Also observed in Table 2, the estimation error of the centre of a uni-modal Gaussian model is about the same as the prediction error of the CNN trained with the least squares error. For further comparisons under the same probabilistic framework, we replace the deterministic CNN with the CNN with a single Gaussian kernel and trained with the negative logarithmic likelihood (denoted as SGN).

4.2.1 Qualitative Analyses

To compare the distributions estimated by different models, 100 samples for each finger tip are drawn from the distributions and scattered in the 3D space where the multiple ground truth skeletons are shown, see Fig. 4. In the third to sixth columns, more details about the distribution shapes are shown by a closer look in two viewpoints, for the samples of the visible index finger tip and occluded ring finger tip.

HMDN is motivated by the intrinsic mapping difference: single-valued mapping for visible and multi-valued mapping for occluded joints. Our results, shown in Fig. 4, demonstrate its ability of modelling this difference by producing interpretable and diverse candidate samples accordingly: samples for visible joints are distributed compact and centred around the ground truth and samples for occluded joints are shaped in their movement range.

In contrast to SGN shown in the top row, whose samples for occluded ring and pinky finger tips are scattered in

a broad sphere range, samples produced by HMDN shown in the bottom row form an arc-shaped region, the movement range within the kinematic constraints. For visible joints, SGN and HMDN produce samples in a compact region while the samples from MDN scatter in a larger region, which may cause difficulty for later stages, generative methods for examples, due to the self-similar appearance of fingers.

With the aid of visibility supervision, HMDN well handles the self-occlusion problem by tailoring different models for respective occasions. The resulting compact distributions that fit both visible joints and occluded joints are important for many hybrid methods. For discriminative-generative pipelines, the distribution largely reduces the space to be explored but also is able to produce diverse candidates to avoid being stuck at local minimas in the generative part. For methods that exploit temporal information and per-frame pose estimation, the distributions of occluded joints estimated by HMDN can be combined with motion information like the speed, direction *etc.* This would give a sharp response at a certain location than uniformly distributed. It is also useful for applications using reinforcement learning to speed up the learning process.

4.2.2 Quantitative Analyses

The superiority of HMDN to SGN and MDN is further supported by the quantitative results demonstrated in Table 2 and Fig. 5, where J is set 10. As almost all prior work uses the euclidean distance of a hypothesis to the ground truth as a measure metric (the distance is in the unit of millimetre), we adopt this euclidean error by following the conversion, but be aware that the metric gives an advantage to SGN as

euclidean errors favour sphere-like distribution.

Table 2: Comparison of models

Model	1 candidate		11 candidates	
	Vis.	Occ.	Vis.	Occ.
Determin	15.1	25.6	-	-
SGN	14.0	25.7	10.0	18.0
MDN	14.6	28.4	9.2	11.7
HMDN	13.6	26.9	8.6	11.3

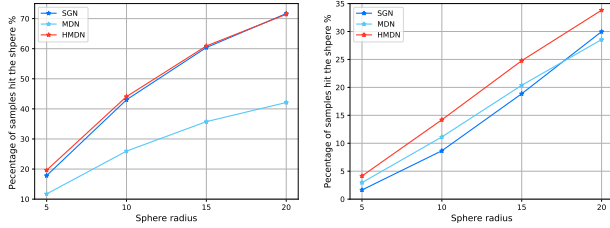


Figure 5: Comparison of percentage of correct samples produced by SGN, MDN and HMDN. Left: visible joints; Right: occluded joints

On one hand, HMDN is able to provide diverse yet interpretable samples for occluded joints as MDN while SGN is not. In Table 2, the centres of the Gaussian kernels of the distributions are used to compare. To demonstrate the diversity, two settings are considered: one kernel from each model is chosen(1 candidate) and all kernels are considered(11 candidates). When only one candidate is to be provided, MDN chooses the maximum modality(with a maximum ratio of π/σ) and HMDN either chooses the single Gaussian kernel or the maximum modality kernel depending on the prediction of the visibility. When all kernels are to be compared, SGN draws more samples from the uni-modal distribution in addition to the kernel centre and when visible, HMDN does the same. The metric is the closest distance to the ground truth among the samples.

For occluded joints, the error drops of MDN and HMDN from 1 candidate to 11 candidates, 16.6mm and 15.6mm respectively, are more than double that of SGN, 6.3mm. This reflects what has been illustrated in Fig. 4: the shapes of the samples of MDN and HMDN are overlaid with the movement range of the predicted joint while the samples of SGN are not as interpretable, scattered in a very large sphere.

On the other hand, HMDN produces samples as compact as SGN does while MDN fails. Though in Table 2, HMDN has the best performance in both 1 candidate and 11 candidates setting under the euclidean error metric, it does not demonstrate the compactness and the improvement from HMDN is marginal. To quantitatively support the compactness as shown in Fig. 4, inspired by the PCK(percentage of correct keypoints) [27] in human pose estimation, we propose percentage of correct samples as the other metric:

the percentage of samples that hits the sphere centred at the ground truth location, which is essentially the integral of the distribution density in the region around the ground truth. 100 samples are drawn and the percentage of samples falling into the sphere with radius from 5mm to 20mm are shown in Fig. 5. The percentage curve for visible joints of HMDN is almost overlapped with that of SGN while that of MDN is lower by a significantly large margin, shown in left in Fig. 5. Despite that the maximum modality of the distribution produced by MDN gives estimations very closer to that of SGN and HMDN, the curves indicate that the variance of the distribution is much higher than SGN and HMDN.

Another observance is that HMDN not just combines the advantages of SGN and MDN but also further improves the advantages of SGN and MDN as shown in Table 2 and Fig. 5. This may be largely due to the visibility supervision, with which HMDN can learn the distribution with models fitting the different data types and results in an easy optimization.

Table 3: Comparison of two HMDN models

Model	Accuracy	TP	TN	FP	FN
HMDN _{hard}	0.878	8.3	10.3	18.0	22.7
HMDN _{soft}	0.875	7.7	10.3	14.7	20.7

4.2.3 Bias

In Section 3.2, we proposed to mitigate the exposure bias during testing by sampling from the visibility variable distribution at training. Table 3 demonstrates its effectiveness by dividing the testing set according to the classification of the visibility variable, *i.e.* true positive(TP), true negative(TN), false positive(FP) and false negative(FN), where "positive" stands for visible joints and "negative" occluded joints, and showing the errors of the four subsets. HMDN trained with the loss functions defined by (9) (10) is denoted by HMDN_{hard} and HMDN trained by (11) (12) is denoted by HMDN_{soft}. The second column is the accuracy of the classification of the visibility variable by two models. For TN and TP, two models obtain similar accuracy while for FP and FN, HMDN_{soft} improves HMDN_{hard} significantly.

4.2.4 Number of Gaussian Kernels

Compared with a standard CNN, HMDN requires one more hyper-parameter, *i.e.* the number of Gaussian kernels. Table 4 compares HMDNs with different number of Gaussian kernels under two settings in Section 4.2.2. When 1 kernel centre is chosen, the increasing number of Gaussian kernels does not improve the estimation and when all the kernel centres are used to be compared, the more number of Gaussian kernels, the lower the error is. The error decrease becomes smaller with more kernels. With more kernels memorizing all data points in the training set, the model is able to

have more modalities at the cost of more number of parameters and may also result in higher variance as experienced in Section 4.2.2 when the model with 11 kernels is compared with the model with 1 kernel for the visible joints.

Table 4: Comparison of HMDN with different numbers of Gaussian Kernels

NumGauss	1 kernel centre		all kernel centres	
	Vis.	Occ.	Vis.	Occ.
11	14.1	27.4	9.3	12.1
31	14.4	27.3	7.6	10.3
51	14.1	27.9	6.7	9.6
71	14.0	28.1	6.6	9.6

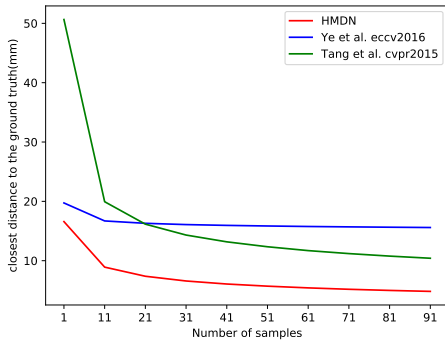


Figure 6: Comparison with prior work on MSHD

4.3. Comparison with the state-of-the-art

It is not straightforward to compare other work because 1) most of the prior-work produces deterministic estimation; 2) frequently used hand pose datasets contain little occlusion as demonstrated in Table 1. As MSHD has a considerable number of occluded joints both in training and testing set, we choose to compare two methods on it. [22, 28] both sample from the discriminative outputs and are able to produce multiple hypotheses. As both methods follow hierarchical structures and have many stages to refine their prediction, to make a fair comparison, we use a CNN network to estimate the global rotation and translation of the hand pose and conditioned on the estimated rotation and translation, HMDN is trained on the dataset.

Ye *et al.* [28] essentially use a deterministic CNN. To produce multiple samples, they jitter around the CNN prediction, which can be treated as a unimodal Gaussian. Tang *et al.* [22] use decision forest to estimate the joint angles and in each leaf node of trees (3 trees in the forest), the data points are modelled by GMM with 3 kernels. During testing, samples are drawn from 3 GMMs from 3 trees, which can be seen as a GMM with 9 kernels.

To make a comparison about the distribution predicted, N samples are drawn and the minimum error to the ground truth among N samples are used to compare. Fig. 6 demon-

strates the change of the minimum error with N . HMDN outperforms both methods significantly. HMDN and Ye *et al.* are both CNN-based methods. When N is 1, the errors of the methods are close, with HMDN a slightly better. However, Ye *et al.* are not able to produce diverse samples to reach lower errors as in HMDN. Though, with GMM, Tang *et al.* are able to providing diverse candidates, the variance of the samples is much higher than HMDN as the errors with smaller numbers of samples are large. From the trend of the error curves in Fig. 6, HMDN demonstrates the superiority of both unimodal Gaussian model and GMM: compact distribution with lower bias and diverse samples.

HMDN has also been evaluated on NYU dataset. Almost all the joints in the training set are visible while on the testing set, there are up to 36% occluded joints. This implies all the joints in the testing dataset will be wrongly predicted as visible joints. Despite the ill-setting for HMDN, the method does not fail but degrades into SGN. Oberweger *et al.* [9] reported the best accuracy, 12.3mm, on the dataset and other errors of prior work listed in [9] range from 13.4mm to 19.8mm. The errors of HMDN and SGN are 16.3mm and 15.9mm.

Table 5: Results on NYU*

Deepproir++		SGN		HMDN	
Vis.	Occ.	Vis.	Occ.	Vis.	Occ.
15.2	12.3	16.8	14.5	16.7	15.6

*The finger joints are compared

5. Conclusion

The paper addresses the occlusion issues in 3D hand pose estimation. Existing discriminative methods are not aware of the multiple modes of occluded joints and thus do not well handle the self-occlusion problem frequently encountered in egocentric-views. The proposed HMDN models the hand pose in a two-level hierarchy to handle visible joints and occluded joints separately according to their unimodal and multi-modal traits. The experiment results show that HMDN adequately models the visible and occluded joints, and significantly outperforms prior work in terms of hand pose estimation accuracy. HMDN also produces interpretable and diverse candidate samples, which is important for hybrid pose estimation methods requiring sampling. As to future work, we consider the improvement by arranging the joints in a tree structure and modelling the distribution for the joint in deeper levels conditioned on the joints in the lower levels. This way, the structure of joints is modelled, and the sampling produces more kinematically valid poses. Testifying HMDN on datasets of hand-object and hand-hand interaction is interesting. Though it was tested on datasets with self-occlusions with one hand, the generalization to different occlusion types is promising.

References

- [1] C. M. Bishop. Mixture density networks. 1994. [2](#)
- [2] C. M. Bishop. *Pattern Recognition and Machine Learning*. 2006. [6](#)
- [3] H. Chang, G. Garcia-Hernando, D. Tang, and T.-K. Kim. Spatio-temporal hough forest for efficient detection-localisation-recognition of fingerwriting in egocentric camera. *CVIU*, 148:87–96, 2016. [1](#)
- [4] C. Constantinopoulos, M. K. Titsias, and A. Likas. Bayesian feature and model selection for gaussian mixture models. *TPAMI*, 28(6):1013–1018, June 2006. [3](#)
- [5] Y. Jang, S.-T. Noh, H. J. Chang, T.-K. Kim, and W. Woo. 3d finger cape: Clicking action and position estimation under self-occlusions in egocentric viewpoint. *IEEE Transactions on Visualization and Computer Graphics (TVCG)*, vol. 21, no. 4, pp.501-510, April 2015, 2015. [1](#)
- [6] D. Kingma and J. Ba. Adam: A method for stochastic optimization. In *ICLR*, 2014. [5](#)
- [7] K. Kinoshita, M. Delcroix, A. Ogawa, T. Higuchi, and T. Nakatani. Deep mixture density network for statistical model-based feature enhancement. In *ICASSP*, 2017. [2](#)
- [8] F. Mueller, D. Mehta, O. Sotnychenko, S. Sridhar, D. Casas, and C. Theobalt. Real-time hand tracking under occlusion from an egocentric rgb-d sensor. In *ICCV*, 2017. [2](#)
- [9] M. Oberweger and V. Lepetit. Deepprior++: Improving fast and accurate 3d hand pose estimation. In *ICCV Workshops*, 2017. [2](#), [8](#)
- [10] M. Oberweger, P. Wohlhart, and V. Lepetit. Training a feedback loop for hand pose estimation. In *ICCV*. [2](#)
- [11] C. Qian, X. Sun, Y. Wei, X. Tang, and J. Sun. Realtime and robust hand tracking from depth. In *ICCV*, 2014. [5](#)
- [12] G. Rogez, J. S. Supancic, and D. Ramanan. First-person pose recognition using egocentric workspaces. In *CVPR*, 2015. [2](#)
- [13] G. Rogez, J. S. Supancic III, M. Khademi, J. M. M. Montiel, and D. Ramanan. 3d hand pose detection in egocentric rgb-d images. In *ECCV Workshops*, 2014. [2](#)
- [14] M. Rohrbach, S. Amin, M. Andriluka, and B. Schiele. A database for fine grained activity detection of cooking activities. In *CVPR*, June 2012. [1](#)
- [15] O. Ronneberger, P. Fischer, and T. Brox. U-net: Convolutional networks for biomedical image segmentation. In *International Conference on Medical Image Computing and Computer-Assisted Intervention*, pages 234–241. Springer, 2015. [5](#)
- [16] T. Sharp, C. Keskin, D. Robertson, J. Taylor, J. Shotton, D. Kim, C. Rhemann, I. Leichter, A. Vinnikov, Y. Wei, D. Freedman, P. Kohli, E. Krupka, A. Fitzgibbon, and S. Izadi. Accurate, robust, and flexible real-time hand tracking. In *CHI*, 2015. [2](#), [5](#)
- [17] S. Sridhar, F. Mueller, A. Oulasvirta, and C. Theobalt. Fast and robust hand tracking using detection-guided optimization. In *CVPR*, 2015. [2](#)
- [18] S. Sridhar, F. Mueller, M. Zollhoefer, D. Casas, A. Oulasvirta, and C. Theobalt. Real-time joint tracking of a hand manipulating an object from rgb-d input. In *ECCV*, 2016. [2](#)
- [19] S. Sridhar, A. Oulasvirta, and C. Theobalt. Interactive markerless articulated hand motion tracking using rgb and depth data. In *ICCV*, 2013. [2](#)
- [20] X. Sun, Y. Wei, S. Liang, X. Tang, and J. Sun. Cascaded hand pose regression. In *CVPR*, 2015. [2](#)
- [21] D. Tang, H.-J. Chang, A. Tejani, and T.-K. Kim. Latent regression forest: Structured estimation of 3D hand posture. In *CVPR*, 2014. [5](#)
- [22] D. Tang, J. Taylor, P. Kohli, C. Keskin, T. K. Kim, and J. Shotton. Opening the black box: Hierarchical sampling optimization for estimating human hand pose. In *ICCV*, 2015. [2](#), [8](#)
- [23] D. Tang, T.-H. Yu, and T.-K. Kim. Real-time articulated hand pose estimation using semi-supervised transductive regression forests. In *ICCV*, 2013. [1](#), [2](#)
- [24] J. Tompson, M. Stein, Y. Lecun, and K. Perlin. Real-time continuous pose recovery of human hands using convolutional networks. *TOG*, 33(5):169, 2014. [1](#), [2](#), [5](#)
- [25] D. Tzionas, L. Ballan, A. Srikantha, P. Aponte, M. Pollefeys, and J. Gall. Capturing hands in action using discriminative salient points and physics simulation. *IJCV*, 118(2):172–193, June 2016. [2](#)
- [26] E. Variani, E. McDermott, and G. Heigold. A gaussian mixture model layer jointly optimized with discriminative features within a deep neural network architecture. In *ICASSP*, 2015. [2](#)
- [27] Y. Yang and D. Ramanan. Articulated human detection with flexible mixtures of parts. *TPAMI*, 35(12):2878–2890, 2013. [7](#)
- [28] Q. Ye, S. Yuan, and T.-K. Kim. Spatial attention deep net with partial pso for hierarchical hybrid hand pose estimation. In *ECCV*, 2016. [2](#), [8](#)
- [29] F. Yin and X. Chai, Xiujuan and Chen. Iterative reference driven metric learning for signer independent isolated sign language recognition. In *ECCV*, 2016. [1](#)
- [30] S. Yuan, Q. Ye, B. Stenger, and T.-K. Kim. Bighand2.2m benchmark: Hand pose data set and state of the art analysis. In *CVPR*, 2017. [2](#), [5](#)
- [31] H. Zen and A. Senior. Deep mixture density networks for acoustic modeling in statistical parametric speech synthesis. In *ICASSP*, 2014. [2](#)